International Journal of Minerals, Metallurgy and Materials
Volume 22, Number 4, April 2015, Page 423
DOI: 10.1007/s12613-015-1089-8

Effect of $CeH_{2.29}$ on the microstructures and hydrogen properties of $LiBH_4$–Mg_2NiH_4 composites

Xin Zhao[1,2], *Shu-min Han*[1,2], *Yuan Li*[1], *Xiao-cui Chen*[1], *and Dan-dan Ke*[1]

1) Hebei Key Laboratory of Applied Chemistry, College of Environmental and Chemical Engineering, Yanshan University, Qinhuangdao 066004, China
2) State Key Laboratory of Metastable Materials Science and Technology, Yanshan University, Qinhuangdao 066004, P. R. China
(Received: 22 July 2014; revised: 11 October 2014; accepted: 13 October 2014)

Abstract: A composite of $LiBH_4$–Mg_2NiH_4 doped with 10wt% $CeH_{2.29}$ was prepared by ball milling followed by dynamic interspace vacuum treatment at 573 K. The introduction of $CeH_{2.29}$ caused a transformation in the morphology of Mg from complex spongy and lamellar to uniformly spongy, resulting in refined particle size and abundant H diffusion pathways. This $LiBH_4$–Mg_2NiH_4 + 10wt% $CeH_{2.29}$ composite exhibited excellent hydrogen storage properties. The starting temperature of rapid H absorption decreased to 375 K in the doped composite from 452 K for the unmodified material, and the onset decomposition temperature of its hydride was reduced from 536 K to 517 K. In addition, the time required for a hydrogen release of 1.5wt% (at 598 K) was 87 s less than that of the un-doped composite.

Keywords: hydrogen storage materials; cerium hydride; mechanical alloying; microstructure

1. Introduction

The challenges of global warming and finite fossil fuel resources have made hydrogen a promising alternative energy source. Hence novel approaches have been focused on metal/intermetallic hydride storage materials. Magnesium is considered as a promising hydrogen storage material for onboard hydrogen storage, especially for vehicular application due to its high hydrogen storage capacity (up to 7.6wt%), light weight and low cost [1]. Nevertheless, its relatively slow hydrogen absorption-desorption kinetic properties and high thermodynamic stability are still key obstacles preventing its practical application [2]. To move this technology forward, researchers have developed several preparation methods such as high-energy ball milling [3], hydriding combustion synthesis (HCS) [4], and arc plasma methods [5]. The grain sizes of MgH_2 ball milled for up to several hours are known to be reduced to nanometer dimensions ranging from 10 to 30 nm [6–8]. As a result, the H-sorption kinetics is substantially accelerated, and the hydrogen desorption temperature is decreased by about 100 K [9]. Since HCS was first developed for the synthesis of Mg_2Ni hydride, it has been also applied to prepare some other Mg-based hydrogen storage materials such as Mg–Ni–Cu alloys [10], Mg–Ni–Fe [11] alloys, and Mg–30wt%$LaNi_5$ composites [12], which presented significantly improved hydrogenation kinetic properties compared to pure MgH_2 powder. Moreover, rare earth elements have also been shown to have positive effects on the hydrogen storage properties of Mg [13]. Long *et al.* [14] reported that an Mg–Ce nanocomposite prepared by arc plasma could absorb 4.07wt% hydrogen at 323 K. The above improvements in hydrogen storage properties generally result from the refined grain size and increased interface between the Mg matrix and additives caused by different preparation methods.

Recently, a new reversible solid-phase reaction involving $LiBH_4$–Mg_2NiH_4 composite was reported [15]. The decomposition products from the original reactants were identified as LiH, MgH_2, $MgNi_{2.5}B_2$, and H_2. Moreover, the dehydrogenation reaction began at 523 K, which was lower than that of the single $LiBH_4$ or Mg_2NiH_4. This improvement makes the composite a potential candidate as a hydro-

Corresponding author: Shu-min Han E-mail: hanshm@ysu.edu.cn

gen storage material. In order to further improve the hydrogen storage properties of the $LiBH_4$–Mg_2NiH_4 composite, Ce hydride was chosen as an additive to accelerate the hydrogen storage kinetics of the composite. The phase transformations and microstructures have been investigated in detail as well as the hydrogen absorption/desorption properties.

2. Experimental

The original Mg_2Ni alloy was prepared by induction melting under the protection of pure argon atmosphere using Mg and Ni ingots (99.9% pure) [16]. The Mg_2Ni alloys were then hydrogenated under a hydrogen pressure of 5 MPa at 673 K for 3 h to ensure complete transformation with respect to Mg_2NiH_4. $LiBH_4$ powder was purchased from Alfa Aesar, and the $CeH_{2.29}$ powder was prepared by hydrogenating Ce metal under a hydrogen pressure of 10 MPa at 773 K. A hydride mixture was prepared by mixing the as-received $LiBH_4$ and Mg_2NiH_4 powders in a mole ratio of 4:5. The mixture was mechanically ball-milled in a stainless steel vial with a ball-to-powder weight ratio of 10:1 using an SPEX 8000 ball milling machine at a speed of 1000 r/min for 2 h. The composite was then heated to 573 K for 2 h under a dynamic interspace vacuum environment to generate Mg. For comparison, a $LiBH_4$–Mg_2NiH_4 + 10wt% $CeH_{2.29}$ composite was prepared by the same ball milling process. In the $CeH_{2.29}$-doped composite, the molar ratio of $LiBH_4$ and Mg_2NiH_4 remained unchanged, and the percentage of $CeH_{2.29}$ was 10wt%. All handing procedures in this work were performed in a glove box filled with purified nitrogen (the concentrations of both oxygen and water were less than 1×10^{-6}) in order to minimize sample contamination.

The hydrogen absorption/desorption properties were measured on a pressure–composition–isotherm (PCI) automatically controlled device (manufactured by Suzuki Shokan in Japan). The temperature programmed desorption (TPD) properties were measured by the PCI device, which was equipped with a homemade programmed heater at a heating rate of 2°/min. In the TPD test, samples were first vacuumed for 10 min to avoid effects of physically absorbed H. Before measurements were performed, each sample was dehydrogenated for 2 h at 623 K and then went through one hydrogen absorption/desorption cycle to be activated. The microstructure was determined via X-ray diffraction (XRD) with Cu K_α radiation and scanning electron microscopy (SEM; HITACHI S3400N). In addition, a high-resolution scanning transmission electron microscope (Cs-corrected STEM; Hitachi H–800) equipped with scanning electron (SE)/bright field (BF)/dark field (DF) was used with an accelerating voltage of 200 kV. The hydrogenated samples were processed in a 3-MPa hydrogen atmosphere at 573 K. The dehydrogenated samples were decomposed in a 0.001-MPa hydrogen atmosphere at 573 K. All the hydrogenated/dehydrogenated samples were collected after hydrogenation characteristic tests.

3. Results and discussion

The XRD patterns in Fig. 1 show the phase transition of the $LiBH_4$–Mg_2NiH_4 composite under different hydrogenation conditions. The XRD pattern of the ball-milled composite shows the obvious broad peaks of Mg_2NiH_4. It is worth mentioning that the Mg_2NiH_4 and $LiBH_4$ mixture was only ground and smashed without chemical reaction during the mechanical ball-milling process. This causes the absence of the $LiBH_4$ diffraction peaks due to their significant grain refinement and amorphous tendency. After the thermal treatment process at 598 K in a dynamic interspace vacuum environment, the Mg_2NiH_4 phase disappears accompanied by the appearance of Mg and $MgNi_{2.5}B_2$ phases (Fig. 1(c)). This transformation is attributed to the reaction between Mg_2NiH_4 and $LiBH_4$, consistent with the results reported by Vajo *et al.* [15]. In the present study, the reaction can be described by reaction (1):

$$4LiBH_4 + 5Mg_2NiH_4 \xrightarrow{573\ K} 2MgNi_{2.5}B_2 + 4LiH + 8Mg + 16H_2 \quad (1)$$

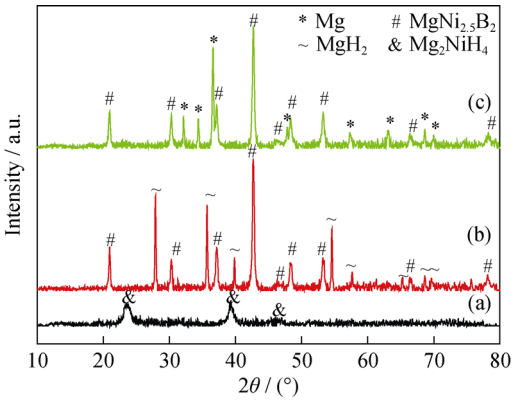

Fig. 1. XRD patterns of the $LiBH_4$–Mg_2NiH_4 composite: (a) after ball milling; (b) hydrogenated; (c) dehydrogenated.

The existence of undecomposed LiH is mainly due to its high thermal stability; its decomposition temperature is over 973 K [17]. The amount of LiH generated by reaction (1) is close to the detection limit of the XRD technique, therefore,

it cannot be observed in Fig. 1(b). In the following hydrogenation process, the Mg in the composite transforms to MgH_2, while the $MgNi_{2.5}B_2$ remains stable (Fig. 1(b)). This indicates that in the following hydrogen absorption/desorption cycles, the hydrogen storage substance in the composite transforms from Mg_2NiH_4 and $LiBH_4$ to MgH_2. For the $LiBH_4$–Mg_2NiH_4 + 10wt% $CeH_{2.29}$ composite (Fig. 2), the $LiBH_4$–Mg_2NiH_4 matrix appears to participate in the above reaction (1), while the stable existing $CeH_{2.29}$ additive does not participate during the hydrogen absorption/desorption processes.

In order to observe the morphology of the $CeH_{2.29}$ additives within the $LiBH_4$–Mg_2NiH_4 composite, SEM images were obtained (Fig. 3). The ball-milled particles of the samples with and without $CeH_{2.29}$ additives exhibit a lamellar structure. However, after hydrogen absorption/desorption cycles, some floccules attached to the smooth surface of the $LiBH_4$–Mg_2NiH_4 composite particles are observed. According to the EDS results in Table 1, the atomic ratio of Mg to Ni in the blocks (marked by "A" in Fig. 4(b)) corresponds to $MgNi_{2.5}B_2$, while the floccules (indicated by "B" in Fig. 4(b)) correspond to Mg enrichment. This indicates that the floccules belong to the Mg generated in reaction (1). Furthermore, the $LiBH_4$–Mg_2NiH_4 + 10wt% $CeH_{2.29}$ composite particles are well covered by flocculent Mg after reaction (1), indicating that the addition of $CeH_{2.29}$ is beneficial to the homogeneous generation of flocculent Mg on the $MgNi_{2.5}B_2$ blocks.

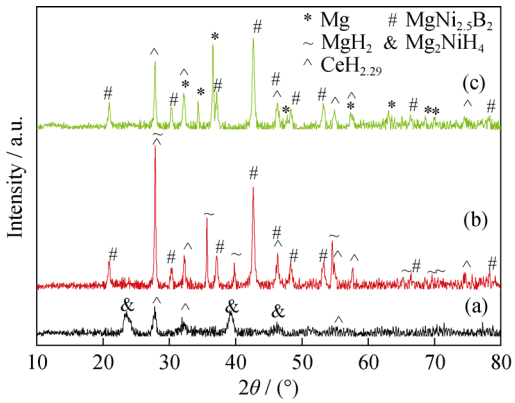

Fig. 2. XRD patterns of the $LiBH_4$–Mg_2NiH_4 + 10wt% $CeH_{2.29}$ composite: (a) after ball milling; (b) hydrogenated; (c) dehydrogenated.

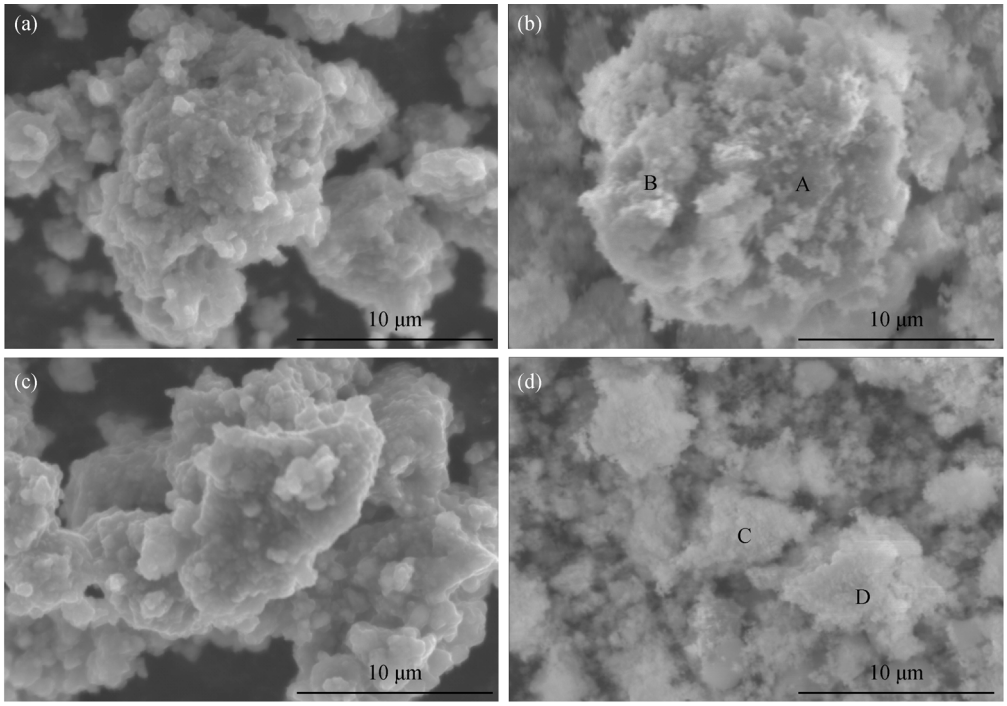

Fig. 3. SEM micrographs: (a) ball-milled and (b) hydrogenated $LiBH_4$–Mg_2NiH_4 composite; (c) ball-milled and (d) hydrogenated $LiBH_4$–Mg_2NiH_4 + 10wt% $CeH_{2.29}$ composite.

Fig. 4 presents the TEM images of the $LiBH_4$–Mg_2NiH_4 and $LiBH_4$–Mg_2NiH_4 + 10wt% $CeH_{2.29}$ composites. After dehydrogenation, the flocculent Mg in the $LiBH_4$–Mg_2Ni composite (Fig. 4(a)) grows along the $MgNi_{2.5}B_2$ particles and shows complex spongy and lamellar structures. However, in the $LiBH_4$–Mg_2NiH_4 + 10wt% $CeH_{2.29}$ composite (Fig. 4(b)), only the spongy morphology is observed, suggesting that the sponge grows outside introversion from the

$CeH_{2.29}$ center. This implies that the reaction of $LiBH_4$ and Mg_2NiH_4 is modified by $CeH_{2.29}$, and that the generated Mg readily forms cellular structures. Meanwhile, the abundant holes in the spongy Mg dramatically decrease the thickness of Mg on the particles and provide abundant interfaces for the contact of Mg and H.

Table 1. EDS results of selected points in Fig. 3 at%

Selected point	Mg	Ni	Ce
A	32.29	67.71	—
B	61.26	38.74	—
C	53.85	36.91	9.24
D	55.64	34.06	10.06

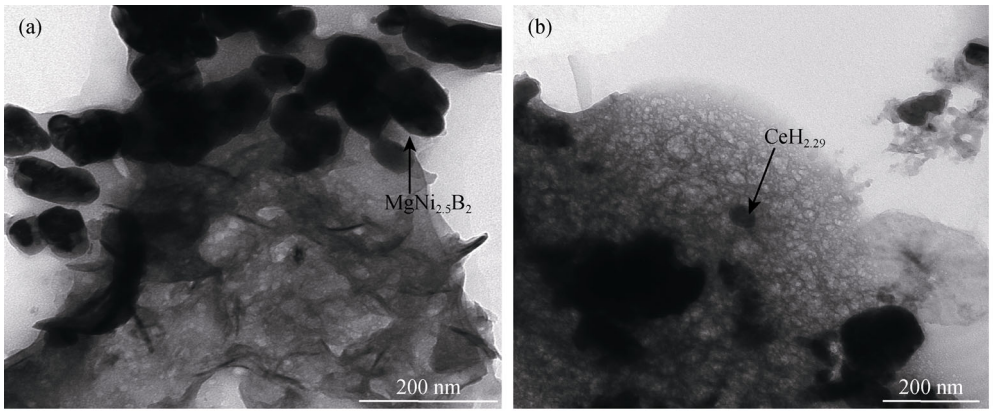

Fig. 4. TEM images of the composites: (a) $LiBH_4$–Mg_2NiH_4; (b)$LiBH_4$–Mg_2NiH_4 + 10wt% $CeH_{2.29}$.

Fig. 5 presents the temperature programmed absorption (TPA) curves of $LiBH_4$–Mg_2NiH_4 with and without $CeH_{2.29}$ additives for comparison. With increasing temperature, the hydrogen storage capacities of the $LiBH_4$–Mg_2NiH_4 and $LiBH_4$–Mg_2NiH_4 + 10wt% $CeH_{2.29}$ composites increase to 2.72wt% and 3.07wt%, respectively. As a hydrogen storage substance, the starting temperature of rapid hydrogen absorption by Mg in the $LiBH_4$–Mg_2NiH_4 + 10wt% $CeH_{2.29}$ composite is 375 K, while that in the $LiBH_4$–Mg_2NiH_4 composite is 452 K. The difference in onset absorption temperature results mainly from the different Mg particle sizes, which affects hydrogen absorption properties. Fig. 6 presents the Fourier transform infrared spectroscopy (FT-IR) spectra of the hydrogenated $LiBH_4$–Mg_2NiH_4 + 10wt% $CeH_{2.29}$ and $LiBH_4$–Mg_2NiH_4 composites. The B–H bond is observed in the spectrum of the hydrogenated $LiBH_4$–Mg_2NiH_4 + 10wt% $CeH_{2.29}$ composite, while it is absent in the spectrum of the $LiBH_4$–Mg_2NiH_4 composite. This indicates that the addition of $CeH_{2.29}$ is beneficial to the regeneration of $LiBH_4$ in the composite, leading to an improvement in its maximum hydrogen storage capacity.

To investigate the dehydrogenation properties of the composites, Fig. 7 shows the hydrogen desorption curves of the $LiBH_4$–Mg_2NiH_4 composites with and without $CeH_{2.29}$. At 548 K, the $LiBH_4$–Mg_2NiH_4 composite releases 0.60wt% hydrogen in 2000 s. With increasing temperature, the hydrogen desorption kinetics of the $LiBH_4$–Mg_2NiH_4 composite improves, with a release of 1.5wt% hydrogen in 532 s at 598 K. The improvement in the samples doped with 10wt%

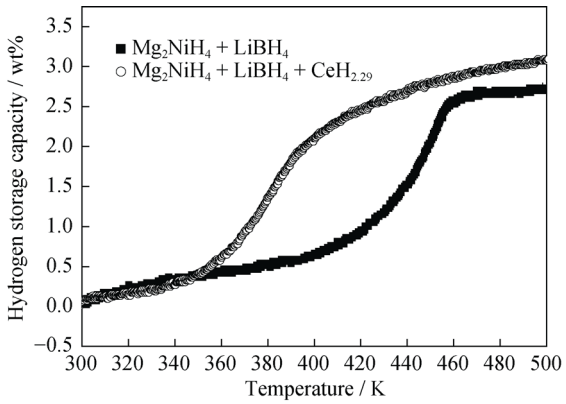

Fig. 5. TPA curves of the $LiBH_4$–Mg_2NiH_4 composites with and without $CeH_{2.29}$.

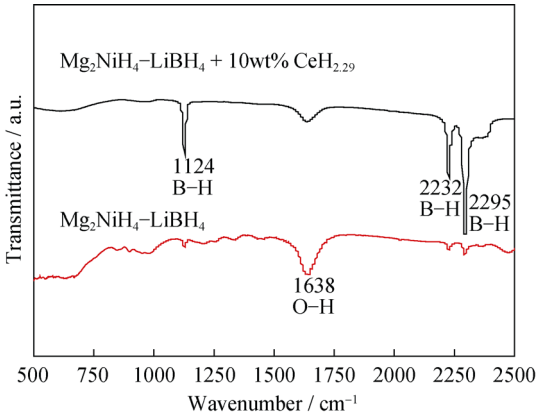

Fig. 6. FT–IR patterns of hydrogenated $LiBH_4$–Mg_2NiH_4 + 10wt% $CeH_{2.29}$ and $LiBH_4$–Mg_2NiH_4 composites.

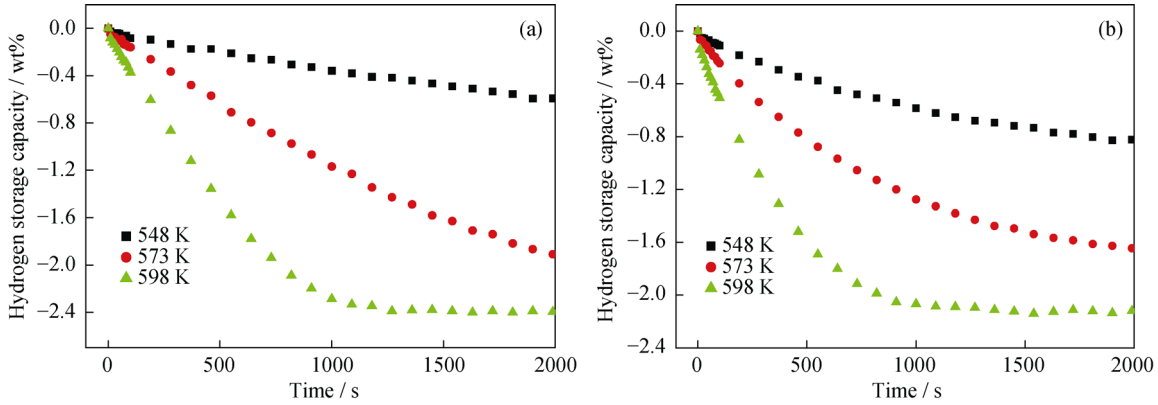

Fig. 7. Hydrogen desorption curves of the composites at different temperatures: (a) $LiBH_4$–Mg_2NiH_4; (b) $LiBH_4$–Mg_2NiH_4 + 10wt% $CeH_{2.29}$.

$CeH_{2.29}$ is obvious, and the hydrogen desorption capacity reaches 0.84wt% within 2000 s at 548 K. Furthermore, the hydrogen desorption capacity at 2000 s reaches 0.84wt%. At 598 K, the hydrogen desorption kinetic properties are significantly improved with a release of 1.5wt% hydrogen in 445 s, 87 s faster compared to the un-doped composite. It is worth mentioning that the finer spongy Mg originating from the $LiBH_4$–Mg_2NiH_4 composite with $CeH_{2.29}$ addition provides more hydrogen diffusion pathways and exhibits better dehydrogenation properties in the tested samples.

To clarify the thermodynamic stabilities of the composites, the TPD curves of the composites are presented in Fig. 8. The generated Mg hydride in the $LiBH_4$–Mg_2NiH_4 + 10wt% $CeH_{2.29}$ composite results in a dramatic decrease in the onset decomposition temperature compared to the $LiBH_4$–Mg_2NiH_4 composite. The onset decomposition temperature of $LiBH_4$–Mg_2NiH_4 + 10wt% $CeH_{2.29}$ composite decreases to 517 K, which is 19 K lower than that of the $LiBH_4$–Mg_2NiH_4 composite and 119 K lower than that of the as-milled MgH_2 powder [18]. Based on reports that decreased Mg particle size can noticeably destabilize its

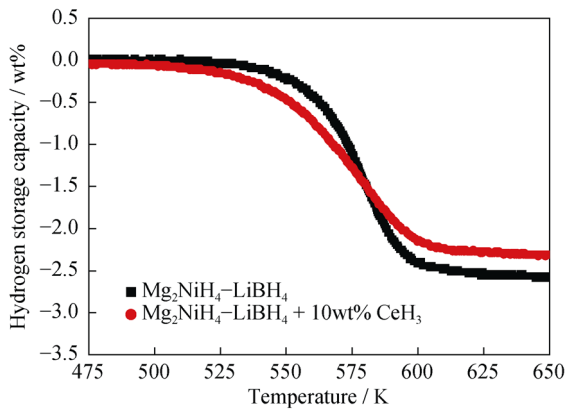

Fig. 8. TPD curves of the $LiBH_4$–Mg_2NiH_4 and $LiBH_4$–Mg_2NiH_4 + 10wt% $CeH_{2.29}$ composites.

hydride, the generated Mg in the $LiBH_4$–Mg_2NiH_4 + 10wt% $CeH_{2.29}$ composite, which has a remarkably small particle size, facilitates the destabilization of its hydride [19] and leads to a lower onset decomposition temperature. Moreover, as the temperature increases to 650 K, the $LiBH_4$–Mg_2NiH_4 + 10wt% $CeH_{2.29}$ composite releases 2.29wt% H, which is 0.28wt% lower than that released by the $LiBH_4$–Mg_2NiH_4 composite. The significant observed improvements can be explained by the following reasons. First, the added $CeH_{2.29}$ exists stably and does not participate in the hydrogen absorption/desorption reaction. Second, the physically-absorbed H in the cellular structure was released before the TPD measurement during vacuuming at room temperature [20].

4. Conclusions

The effects of $CeH_{2.29}$ on the microstructure and hydrogen storage properties of the $LiBH_4$–Mg_2NiH_4 composite were investigated. The SEM results indicated that the addition of $CeH_{2.29}$ was beneficial to the homogeneous generation of flocculent Mg on $MgNi_{2.5}B_2$ blocks. In the $LiBH_4$–Mg_2NiH_4 + 10wt% $CeH_{2.29}$ composite, the generated Mg presented a uniformly spongy microstructure, while Mg in the $LiBH_4$–Mg_2NiH_4 composite showed a complex morphology with spongy and lamellar structures. The composite doped with $CeH_{2.29}$ exhibited a significant decrease in the onset decomposition temperature; this temperature reached 517 K, which was 19 K lower than that of the $LiBH_4$–Mg_2NiH_4 composite. Meanwhile, the time to release 1.5wt% hydrogen (at 598 K) for the $LiBH_4$–Mg_2NiH_4 + 10wt% $CeH_{2.29}$ composite hydride was 445 s, 87 s faster than that of the un-doped composite.

Acknowledgements

This research was financially supported by the National

Natural Science Foundation of China (No. 50971112), the Natural Science Foundation of Hebei Province (No. E2010001170), and the Scientific Research Projects in Colleges and Universities in Hebei Province, China (No. ZD2014004).

References

[1] P. Selvam, B. Viswanathan, C.S. Swamy, and V. Srinivasan, Magnesium and magnesium alloy hydrides, *Int. J. Hydrogen Energy*, 11(1986), No. 3, p. 169.

[2] N.V. Mushnikov, A.E. Ermakov, M.A. Uimin, V.S. Gaviko, P.B. Terent'ev, A.V. Skripov, A.P. Tankeev, A.V. Soloninin, and A.L. Buzlukov, Kinetics of interaction of Mg-based mechanically activated alloys with hydrogen, *Phys. Met. Metallogr.*, 102(2006), No. 4, p. 421.

[3] R.A. Varin, M. Jang, T. Czujko, and Z. Wronski, The effect of ball milling under hydrogen and argon on the desorption properties of MgH_2 covered with a layer of $Mg(OH)_2$, *J. Alloys Compd.*, 493(2010), No. 1-2, p. L29.

[4] L.Q. Li, T. Akiyama, and J. Yagi, Activation behaviors of Mg_2NiH_4 at different hydrogen pressures in hydriding combustion synthesis, *Int. J. Hydrogen Energy*, 26(2001), No. 10, p. 1035.

[5] J.X. Zou, X.Q. Zeng, Y.J. Ying, X. Chen, H. Gao, S. Zhou, and W.J. Ding, Study on the hydrogen storage properties of core–shell structured Mg–RE (RE = Nd, Gd, Er) nano-composites synthesized through arc plasma method, *Int. J. Hydrogen Energy*, 38(2013), No. 5, p. 2337.

[6] M. Danaie and D. Mitlin, TEM analysis and sorption properties of high-energy milled MgH_2 powders, *J. Alloys Compd.*, 476(2009), No. 1-2, p. 590.

[7] V. Fuster, G. Urretavizcaya, and F.J. Castro, Characterization of MgH_2 formation by low-energy ball-milling of Mg and Mg + C (graphite) mixtures under H_2 atmosphere, *J. Alloys Compd.*, 481(2009), No. 1-2, p. 673.

[8] M. Porcu, A.K. Petford-Long, and J.M. Sykes, TEM studies of Nb_2O_5 catalyst in ball-milled MgH_2 for hydrogen storage, *J. Alloys Compd.*, 453(2008), No. 1-2, p. 341.

[9] M. Polanski, J. Bystrzycki, and T. Plocinski, The effect of milling conditions on microstructure and hydrogen absorption/desorption properties of magnesium hydride (MgH_2) without and with Cr_2O_3 nanoparticles, *Int. J. Hydrogen Energy*, 33(2008), No. 7, p. 1859.

[10] L.Q. Li, I. Saita, K. Saito, K. Saito, and T. Akiyama, Hydriding combustion synthesis of hydrogen storage alloys of Mg–Ni–Cu system, *Intermetallics*, 10(2002), No. 10, p. 927.

[11] I. Saita, K. Saito, and T. Akiyama, Hydriding combustion synthesis of $Mg_2Ni_{1-x}Fe_x$ hydride, *J. Alloys Compd.*, 390(2005), No. 1-2, p. 265.

[12] H. Gu, Y.F. Zhu, and L.Q. Li, Hydrogen storage properties of Mg–30wt.% $LaNi_5$ composite prepared by hydriding combustion synthesis followed by mechanical milling (HCS + MM), *Int. J. Hydrogen Energy*, 34(2009), No. 3, p. 1405.

[13] L.C. Pei, S.M. Han, J.S. Wang, L. Hu, X. Zhao, and B.Z. Liu, Hydrogen storage properties and phase structures of RMg_2Ni (R = La, Ce, Pr, Nd) alloys, *Mater. Sci. Eng. B*, 177(2012), No. 18. p. 1589.

[14] S. Long, J.X. Zou, Y.N. Liu, X.Q. Zeng, and W.J. Ding, Hydrogen storage properties of a Mg–Ce oxide nano-composite prepared through arc plasma method, *J. Alloys Compd.*, 580(2013), No. Suppl., p. 167.

[15] J.J. Vajo, W. Li, and P. Liu, Thermodynamic and kinetic destabilization in $LiBH_4/Mg_2NiH_4$: promise for borohydride-based hydrogen storage, *Chem. Commun.*, 46(2010), No. 36, p. 6687.

[16] X. Zhao, S.M. Han, X.L. Zhu, B.Z. Liu, and Y.Q. Liu, Investigations on hydrogen storage properties of $Mg_2Ni + x$ wt% $LaMg_2Ni$ (x = 0, 10, 20, 30) composites, *J. Solid State Chem.*, 190(2012), p. 68.

[17] A.H. Reshak, MgH_2 and LiH metal hydrides crystals as novel hydrogen storage material: electronic structure and optical properties, *Int. J. Hydrogen Energy*, 38(2013), No. 27, p. 11946.

[18] Y.H. Jia, S.M. Han, W. Zhang, X. Zhao, P.F. Sun, Y.Q. Liu, H. Shi, and J.S. Wang, Hydrogen absorption and desorption kinetics of MgH_2 catalyzed by MoS_2 and MoO_2, *Int. J. Hydrogen Energy*, 38(2013), No. 5, p. 2352.

[19] S. Cheung, W.Q. Deng, A.C. van Duin, and W.A. Goddard, $ReaxFF_{MgH}$ reactive force field for magnesium hydride systems, *J. Phys. Chem. A*, 109(2005), No. 5, p. 851.

[20] A.M. Rashidi, A. Nouralishahi, A.A. Khodadadi, Y. Mortazavi, A. Karimi, and K. Kashefi, Modification of single wall carbon nanotubes (SWNT) for hydrogen storage, *Int. J. Hydrogen Energy*, 35(2010), No. 17, p. 9489.